Flow Control of $A + B \to C$ Fronts by Radial Injection

Fabian Brau,* G. Schuszter,† and A. De Wit‡
Université libre de Bruxelles (ULB), Nonlinear Physical Chemistry Unit, CP231, 1050 Brussels, Belgium
(Received 31 December 2016; revised manuscript received 23 February 2017; published 31 March 2017)

The dynamics of $A + B \to C$ fronts is analyzed theoretically in the presence of passive advection when A is injected radially into B at a constant inlet flow rate Q. We compute the long-time evolution of the front position, r_f, of its width, w, and of the local production rate R of the product C at r_f. We show that, while advection does not change the well-known scaling exponents of the evolution of corresponding reaction-diffusion fronts, their dynamics is however significantly influenced by the injection. In particular, the total amount of product varies as $Q^{-1/2}$ for a given volume of injected reactant and the front position as $Q^{1/2}$ for a given time, paving the way to a flow control of the amount and spatial distribution of the reaction front product. This control strategy compares well with calcium carbonate precipitation experiments for which the amount of solid product generated in flow conditions at fixed concentrations of reactants and the front position can be tuned by varying the flow rate.

DOI: 10.1103/PhysRevLett.118.134101

Reaction-diffusion (RD) fronts are ubiquitous in a wide variety of phenomena ranging from population dynamics [1,2], disease spreading [3,4], and biological pattern formation [5] to image processing [6] and nanotechnology [7,8] to name a few. Among the large family of RD fronts, $A + B \to C$ fronts are observed when initially separated reactants A and B meet by diffusion and react to produce C. Depending on the nature of A and B, their dynamics is representative of many problems in chemistry [9], geochemistry [10], finance [11], particle physics [12], and many others. The temporal evolution of the front position, x_f, defined as the location of maximum C production, of the front width w, and of the local production rate, $R(x_f)$, has long been derived theoretically [13,14] and confirmed experimentally [15–17]. The related scalings $x_f \sim t^{1/2}$, $w \sim t^{1/6}$, and $R(x_f) \sim t^{-2/3}$ form the basis of $A + B \to C$ RD front theory confirmed in many applications.

In flows, $A + B \to C$ processes provide another important class of dynamics, e.g., in combustion [18], atmospheric chemistry [19], and ecological [20,21] or environmental problems [22]. The coupling between convection and reaction leads to complex dynamics when the flow, actively influenced by transported species, feedbacks on their spatiotemporal distribution [23–25].

The radial advection of reacting species is currently receiving growing attention. For example, $A + B \to C$-type precipitation reactions in a radial flow give rise to a large variety of self-assembled structures [26–29], to thermodynamically unstable crystalline forms [30], or to compositions different from those obtained in homogeneous systems [31–34]. Similarly, a suitable redefinition of distance may recast some transport phenomena into a radial spreading as done in studies of infectious disease spreading [35].

Motivated by the broad applications of radial transport in reactive systems, we analyze both theoretically and experimentally the properties of reaction-diffusion-advection (RDA) fronts obtained when a $A + B \to C$ reactive miscible interface is subjected to a passive radial advection. We show that even though the classical RD scalings are maintained, the flow affects the proportionality coefficients, the total amount of product generated in space and time, and the front position, which paves the way to a flow control of the front dynamics.

Let us consider a two-dimensional system in which a species A in concentration A_0 is injected radially at a constant flow rate Q into a domain initially filled with B in concentration B_0. Upon contact, A and B react to produce C. All three species are transported by both diffusion and passive advection. In a rectilinear geometry, advection at a constant velocity perpendicular to the front does not affect the dynamics in a frame moving with the advection speed. In a radial geometry, the RD problem does not admit a sustained front solution as a point source with a constant concentration A_0 cannot be maintained in the presence of diffusion. The situation is however different in the case of a constant injection of A at a given localized feeding point. The chemicals are then advected by a radial velocity field, $v_r = Q/r$. We assume that v_r is not modified by the reaction, and that the displacement is hydrodynamically stable and preserves the radial symmetry; i.e., the variables depend only on the radial coordinate, r, and on time, t. In cylindrical coordinates (r, θ, z), the equations governing this dynamics are then

$$\partial_t a + v_r \partial_r a = (\partial_r^2 + r^{-1}\partial_r)a - ab, \tag{1a}$$

$$\partial_t b + v_r \partial_r b = (\partial_r^2 + r^{-1}\partial_r)b - ab, \tag{1b}$$

$$\partial_t c + v_r \partial_r c = (\partial_r^2 + r^{-1}\partial_r)c + ab, \tag{1c}$$

where $a(r,t)$, $b(r,t)$, and $c(r,t)$ are, respectively, the concentrations of the reactants A, B and product C normalized by A_0. Time and space have been rescaled by $\tau = 1/kA_0$ and $\ell = (D\tau)^{1/2}$, respectively, where k is the reaction kinetic constant and D is the diffusion coefficient assumed equal for all species, since this assumption does not affect the asymptotic scaling properties [14,36]. The production rate of C is defined as $R(r,t) = a(r,t)b(r,t)$. An example of the concentration profiles a and b and of the production rate R obtained by solving Eqs. (1) numerically is shown in Fig. 1(a).

Subtracting Eqs. (1b) from (1a) and performing the change of variables $\eta = r^2/(4t)$ leads to an equation for $u = a - b$,

$$\partial_\eta^2 u + \left(1 + \frac{1 - Q/2}{\eta}\right)\partial_\eta u = 0. \tag{2}$$

The BCs are $u = 1$ for $r \to 0$ where $b = 0$ and $a = 1$, and $u = -\gamma$ for $r \to \infty$ where $a = 0$ and $b = B_0/A_0 = \gamma$. The solution of Eq. (2) satisfying these BCs reads

$$u(r,t) = -\gamma + (1+\gamma)\mathcal{Q}[Q/2, r^2/(4t)], \tag{3}$$

where $\mathcal{Q}(a,x) = \Gamma(a,x)/\Gamma(x)$, $\Gamma(a,x)$, and $\Gamma(x) = \Gamma(0,x)$ are the regularized, incomplete, and complete gamma functions, respectively [37]. Note that, in the absence of flow ($Q = 0$), the general solution of Eq. (2) is singular at $r = 0$, a sign that a radial RD front cannot be sustained only by diffusion of A from a point. In the presence of a flow, the position of the reaction front, r_f, defined as the point where $u = 0$, is obtained from Eq. (3),

$$r_f = 2\sqrt{\mathcal{K}t}, \quad \text{with} \quad \mathcal{K} = \mathcal{Q}^{-1}\left(Q/2, \frac{\gamma}{1+\gamma}\right), \tag{4}$$

where $\mathcal{Q}^{-1}(a,x)$ is the unique solution for y of the equation $x = \mathcal{Q}(a,y)$ ($x \le 1$, $a > 0$, and $y \ge 0$). When $\gamma \simeq 1$ and $Q \gg 1$, Eq. (4) simplifies to [38]

$$r_f \simeq 2\sqrt{t}\left(\frac{Q}{2} + \frac{1-\gamma}{1+\gamma}\frac{\sqrt{\pi Q}}{2}\right)^{1/2}. \tag{5}$$

Equation (5) implies that when $\gamma = 1$, the motion of the RDA front is simply governed by volume conservation, $r_f(t) \sim (Qt)^{1/2}$. When $\gamma \neq 1$, the front lags behind ($\gamma > 1$) or moves faster ($\gamma < 1$) than the reference advection case obtained for $\gamma = 1$.

To obtain the asymptotic production rate R and width w of the reaction zone, we substitute $b = a - u$ into Eq. (1a) to obtain

$$\partial_t a = \left(\partial_r^2 + \frac{1-Q}{r}\partial_r\right)a - a^2 + ua. \tag{6}$$

Even if this nonlinear partial differential equation cannot be solved in general, the derivation of scaling laws is nevertheless possible if, following [13], we assume that the front width w increases with time not faster than the depletion zone $W_d \sim Q^{1/4}t^{1/2}$; see Fig. 1(a) and [38]. This means that, in the long time limit, w is negligible compared to W_d. Expanding $u(r,t)$ given by Eq. (3) around r_f, we obtain

$$u(r,t) = -K(r - r_f)/\sqrt{t} + \mathcal{O}[(r-r_f)^2/t], \tag{7a}$$

$$K(Q,\gamma) = (1+\gamma)[\Gamma(Q/2)]^{-1}\mathcal{K}^{(Q-1)/2}e^{-\mathcal{K}}, \tag{7b}$$

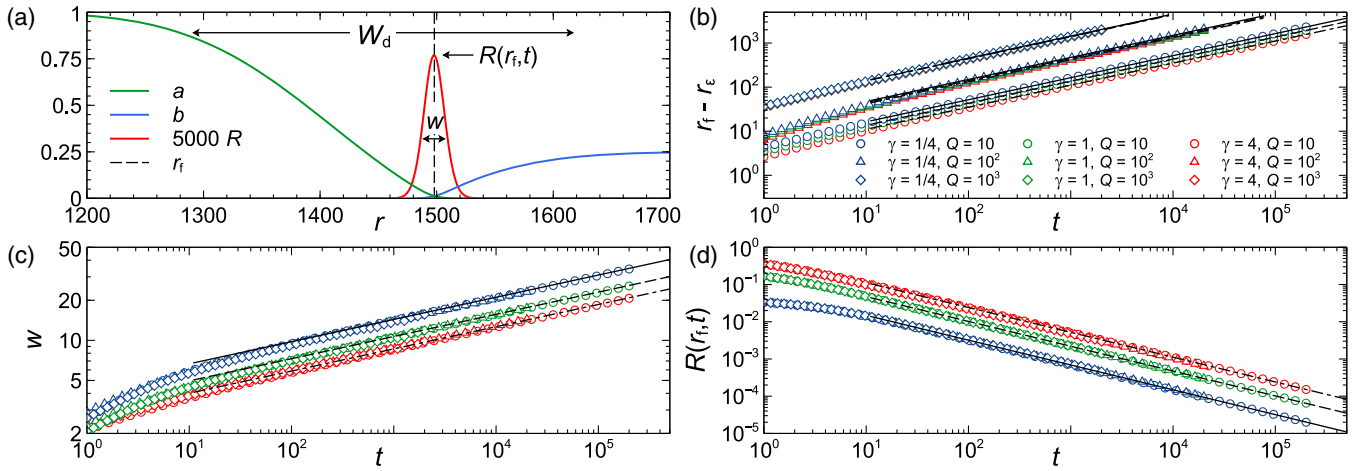

FIG. 1. (a) Numerical concentration profiles of A and B, front position r_f, width w, local production rate $R(r_f,t)$, and depletion zone W_d at $t = 10^4$ for $Q = 100$, $\gamma = 1/4$. The numerical integration has been performed in the interval $[r_\epsilon = 1, r_{\max} = 3500]$ with initial conditions $a(r,0) = H(r_\epsilon - r)$, $b(r,0) = \gamma H(r - r_\epsilon)$, $c(r,0) = 0$, where $H(x)$ is the Heaviside function, and boundary conditions (BC) $a(r_\epsilon,t) = 1, a(r_{\max},t) = b(r_\epsilon,t) = 0, b(r_{\max},t) = \gamma, c(r_\epsilon,t) = c(r_{\max},t) = 0$. BC are set at $r = r_\epsilon$ instead of $r = 0$ to avoid the apparent singularity. Temporal evolution of r_f (b), w (c), and $R(r_f,t)$ (d) for $Q = 10$, 10^2, 10^3 and $\gamma = 1/4$, 1, 4. The symbols correspond to the numerical solutions while the solid ($\gamma = 1/4$), dashed ($\gamma = 1$), and dash-dotted ($\gamma = 4$) lines correspond to Eqs. (4) and (8).

$$\underset{Q\gg 1}{\simeq}[2\ln(1+\gamma/\sqrt{2\pi})]^{1/2}. \tag{7c}$$

Figures 2(a) and 2(b) show the variation of K with respect to Q and γ. For Q large enough, K is essentially independent on Q. Outside the reaction front in the region $r < r_f$, $a = u$ since $b = 0$ whereas in the region $r > r_f$, $a = 0$. Using the ansatz $a(r,t) = t^{-\omega_1/2}G(z)$ with $z = (r - r_f)/t^{\omega_2}$, the above BC together with Eq. (7a) impose $G(z) \to -Kz$ for $z \to -\infty$, $G(z) = 0$ for $z \to \infty$, and $\omega_2 + \omega_1/2 = 1/2$. Substituting this ansatz into Eq. (6) and requiring that the term $d_z^2 G(z)$ remains in the scaling limit $t \to \infty$ while keeping z fixed, we find $\omega_2 = 1/6$ ($\omega_1 = 2/3$) and $d_z^2 G(z) = G^2(z) + KzG(z)$. The scaling function G is thus the same as in a rectilinear geometry without advection [13]; only K differs. Therefore, the asymptotic expressions of the width of the reaction zone, w, and of the local production rate, R, are given by [13]

$$w(t) \simeq \pi K^{-1/3} t^{1/6}, \qquad R(r_f,t) \simeq \frac{29}{\pi^4} K^{4/3} t^{-2/3}. \tag{8}$$

Equations (4) and (8) show that the classical RD scaling exponents are thus recovered in the RDA system and are not affected by a passive radial advection. The coefficients $\mathcal{K}$ and K depend however on Q, which evidences the possibility of controlling the properties of $A + B \to C$ fronts in radial flows by tuning the flow rate.

Figures 1(b)–1(d) show a comparison between the scalings (4) and (8) and numerical solutions of Eqs. (1). The effect of γ on the front position is more pronounced for low flow rates. This effect and the ordering of the curves in Fig. 1(b) can be simply understood from Eq. (5). Figures 1(c) and 1(d) show that w and R do not depend significantly on the flow rate because the coefficient K is almost constant once Q is large enough; see Figs. 2(a) and 2(b). However, because $r_f \sim (Qt)^{1/2}$, the value of R and w at a given radial distance from the injection point varies with Q: $R \sim Q^{2/3} r_f^{-4/3}$ and $w \sim Q^{-1/6} r_f^{1/3}$ for $Q \gg 1$. The yield and spatial distribution of the product can thus be controlled by the flow rate.

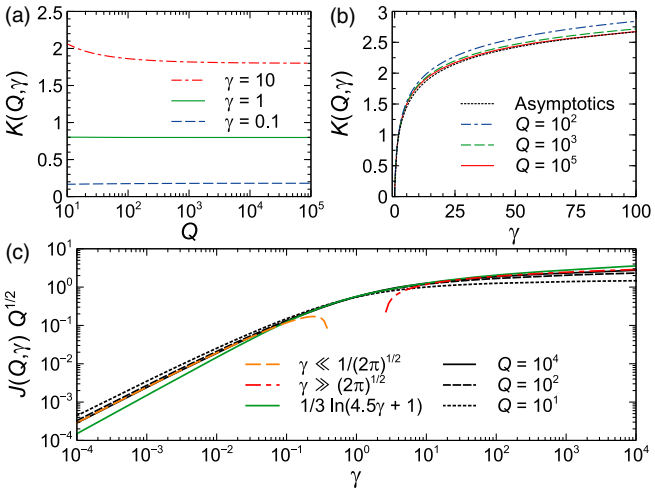

FIG. 2. (a) K as a function of Q for three values of γ. (b) K as a function of γ for three values of Q together with the asymptotic expression (7c). (c) Evolution of $J(Q,\gamma)Q^{1/2}$, see Eq. (10), as a function of γ for several values of Q. The asymptotic behaviors for small and large values of γ are also shown together with an approximate expression.

Similarly, it can be shown that the total amount n_C of product as a function of time, defined as $n_C(t) = \int c(r,t)d\boldsymbol{r}$, reduces to [38]

$$n_C(t) \sim K(Q,\gamma)\mathcal{K}(Q,\gamma)^{1/2} t \underset{Q\gg 1}{\sim} Q^{1/2} t. \tag{9}$$

Asymptotically, n_C grows thus linearly with time and, for a given time, grows as $Q^{1/2}$. This contrasts with the RD scaling in rectilinear geometry, $n_C \sim t^{1/2}$, which highlights the interest of flow conditions to control the yield of $A + B \to C$ processes.

To test our theoretical predictions experimentally, it is useful to express our results in dimensional variables noted with a bar. Assuming a radial injection in a solution layer of thickness $\bar{h}$ and noting that, from volume conservation, $\bar{Q}\,\bar{t} = \pi \bar{r}^2 \bar{h}$, we obtain the radial velocity field, $\bar{v}_r = (\ell/\tau)v_r = d\bar{r}/d\bar{t} = \bar{Q}/(2\pi\bar{h}r\ell)$ with $Q = \bar{Q}/(2\pi\bar{h}D)$, the Péclet number of the problem. Since the time scale of an experiment depends on the flow rate, it is useful to express Eq. (9) as a function of the injected volume $\bar{V} = \bar{Q}\,\bar{t}$,

$$\bar{n}_C(\bar{V}) \sim A_0 J(Q,\gamma)\bar{V} \underset{Q\gg 1}{\sim} A_0 j(\gamma)(\bar{Q}/D\bar{h})^{-1/2}\bar{V}, \tag{10}$$

where $\bar{n}_C = A_0 \ell^3 n_C$ and $j = \lim_{Q\to\infty} J(Q,\gamma)Q^{1/2}$ where $J = K\mathcal{K}^{1/2}Q^{-1}$. Indeed, for $Q \gg 1$, Fig. 2(c) shows that the function J factorizes as $J = j(\gamma)Q^{-1/2}$. The function j behaves like $\gamma[\ln(1/(\gamma\sqrt{2\pi}))]^{1/2}$ for $\gamma \ll 1/\sqrt{2\pi}$ and like $[\ln(\gamma/\sqrt{2\pi})]^{1/2}$ for $\gamma \gg \sqrt{2\pi}$; see Fig. 2(c). In good approximation, especially for $0.1 < \gamma < 10$, j can be written as

$$j(\gamma) \simeq [\ln(4.5\gamma + 1)]/3. \tag{11}$$

$\bar{n}_C$ varies thus logarithmically with $\gamma = B_0/A_0$ whereas it varies as a power of $\bar{Q}$. Equation (10), valid asymptotically when $\bar{V}$ is large enough, shows that

$$\bar{n}_C = \beta(\bar{Q},\gamma)\bar{V} + \delta(\bar{Q},\gamma), \qquad \beta \underset{Q\gg 1}{\sim} A_0 j(\gamma)\bar{Q}^{-1/2}. \tag{12}$$

To test prediction (12), experiments are performed with an $A + B \to C$ precipitation reaction by radial injection in a confined reactor of a solution of carbonate ions ($A = CO_3^{2-}$) into a solution of calcium ions ($B = Ca^{2+}$) to yield the solid calcium carbonate product ($C = CaCO_3$)

[see Fig. 3(a) and [28,29]]. Experiments are performed at concentrations $0.2\ \mathrm{M} \leq A_0,\ B_0 \leq 0.4\ \mathrm{M}$ and flow rates, $0.01\ \mathrm{mL/min} \leq \bar{Q} \leq 0.1\ \mathrm{mL/min}$, to limit convection and the formation of complex patterns observed at larger concentrations or flow rates [28,29]. The corresponding dimensionless flow rates ($50 \lesssim Q \lesssim 500$) are nevertheless large enough to reach the asymptotic regime of β. The viscosity ratio between the two fluids ($\mu_{Na_2CO_3}/\mu_{CaCl_2} < 1.2$) and the change in permeability are too small to produce fingering with such flow rates [42,43]. A representative spatially homogeneous and radially symmetric precipitate obtained in such conditions is shown in Fig. 3(b). Figures 3(c)–3(e) show the distribution of precipitate particles at various distances from the injection point. The size of the particles is rather insensitive to the concentrations and flow rates and is about $d_p = 6\ \mu$m [38]. The area covered by the particles varies between 2% and 12% of the field of view areas depending on the concentrations, flow rate, and distance from the inlet. The mean nearest neighbor distance is indeed about $2.5d_p$ [38]. There is thus almost no overlap between particles and the total amount of light $I_{tot} = I\int_0^\infty N(A_p)dA_p$ they reflect can be used as a quantitative measure of the amount of solid product. Here I is the amount of reflected light per unit area and $N(A_p)$ is the number of particles of area A_p. The width of this distribution is essentially constant and its amplitude is proportional to the total number of particles, N_{tot} [38]. The total grey scale intensity of the pattern, I_{tot}, is therefore a measure of the total amount of precipitate, $I_{tot} \sim N_{tot} \sim \bar{n}_C$. It is thus expected to scale like (12) after some transient regime with a slope β' proportional to β. I_{tot} is measured as the sum of the grey scale intensity of each pixel of the pattern (see [28,38]).

Figure 4(a) shows I_{tot} averaged on at least three experiments as a function of the injected volume $\bar{V}$ of the carbonate solution for $\gamma = 1$ and $A_0 = 0.2$ M (see [38] for other γ). After some transient, I_{tot} grows linearly with $\bar{V}$, in agreement with Eq. (12), with slopes $\beta' \sim \beta \sim \bar{Q}^{-0.4}$ as shown in Fig. 4(b), i.e., with an exponent close to the predicted one. The production of calcium carbonate decreases thus slightly less compared to the theoretical prediction when $\bar{Q}$ increases. This may result from undetected buoyancy-driven convection due to the slight density difference between the precipitate and ion solutions, which enhances the mixing and hence the production of precipitate. The ordering of the curves shown in Fig. 4(b) when γ is varied follows the predicted one since the coefficient $A_0 j(\gamma)$, see Eqs. (11) and (12), satisfies the inequalities $0.2j(1) < 0.2j(2) < 0.4j(1/2)$. The theory predicts however a smaller difference between the curves for $\gamma = 1/2$ and $\gamma = 2$.

We have thus shown that the amount of precipitate can be tuned by the flow rate with scalings in good agreement with theory. Similarly, the scaling for the front position, r_f, can be tested. In dimensional form, Eq. (4) reads $\bar{r}_f = \mathcal{R}(\bar{t}/\bar{h})^{1/2}$ with $\mathcal{R} = [(2\mathcal{K}/Q)(\bar{Q}/\pi)]^{1/2}$ and where

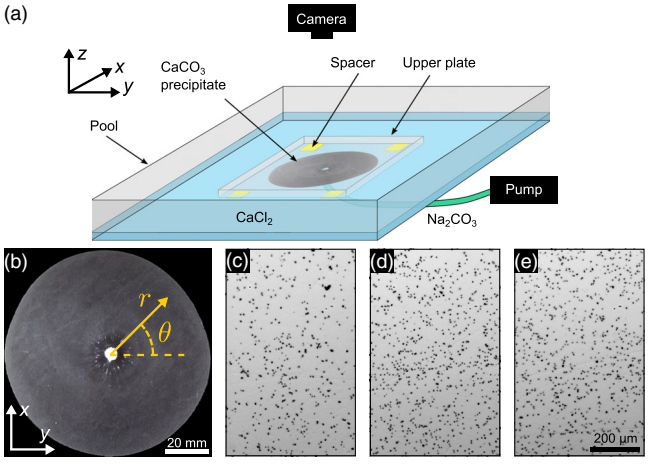

FIG. 3. (a) Schematic of the experimental setup. (b) Representative precipitate distribution obtained by injecting radially, at a flow rate $\bar{Q} = 0.1$ mL/min, an aqueous solution of sodium carbonate 0.4 M into an aqueous solution of calcium chloride 0.2 M confined between two Plexiglas plates separated by a gap $\bar{h} = 0.5$ mm. [(c)–(e)] Optical microscope images of the precipitate taken at 2 (c), 3 (d), and 4 cm (e) from the injection point.

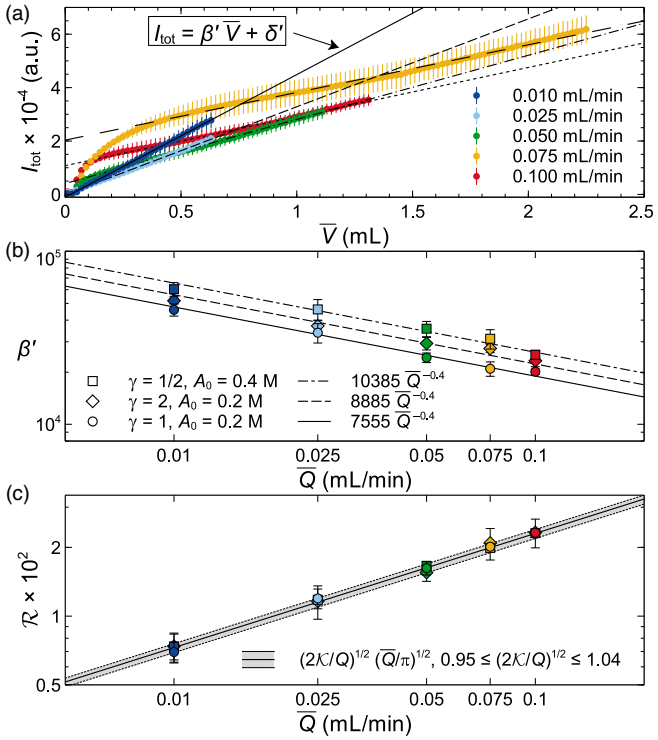

FIG. 4. (a) I_{tot} as a function of the volume $\bar{V}$ of the injected CO_3^{2-} solution for various $\bar{Q}$ and $A_0 = B_0 = 0.2$ M. (b) Slope β' of the asymptotic linear regime shown in (a) as a function of $\bar{Q}$ for several γ. (c) Coefficient $\mathcal{R}$, defined in the text and expressed in $(\mathrm{cm}^3/\mathrm{s})^{1/2}$, as a function of $\bar{Q}$.

$0.95 \leq (2\mathcal{K}/Q)^{1/2} \leq 1.04$ for $50 \leq Q \leq 500$ and $1/2 \leq \gamma \leq 2$ [38]. The influence of γ on the front position is therefore marginal. The coefficient $\mathcal{R}$ has been extracted from the experimental images by tracking $\bar{r}_f$ as a function $\bar{t}$ for various $\bar{Q}$ and γ [38]. The variation of $\mathcal{R}$ with $\bar{Q}$ compares well with theory; i.e., the front position scales as $\bar{r}_f \simeq (\bar{Q}\,\bar{t})^{1/2}$ [see Fig. 4(c)].

We have shown theoretically and confirmed experimentally on a precipitation system that a passive radial advection can affect the dynamics of $A + B \to C$ fronts. The well-known RD scalings $r_f \sim t^{1/2}$, $w \sim t^{1/6}$, and $R \sim t^{-2/3}$ are recovered in the presence of the flow, yet with coefficients that depend on the injection flow rate. After a short transient, the amount of product increases linearly with the injected volume with a slope that depends on the flow rate. This shows that hydrodynamic flows can conveniently be used to tune the amount and spatial distribution of the product of the reaction. These results generalize to flow conditions the classical scalings of reaction-diffusion $A + B \to C$ fronts known since the founding article by Gálfi and Rácz [13]. Because of the genericity of such fronts, our results pave the way to their control by flows in a wide range of applications depending on the adequate interpretation of the advection term and of the nature of A and B.

The authors thank Prodex for financial support.
F. B. and G. S. contributed equally to this work.

*fabian.brau@ulb.ac.be
†Present address: Department of Physical Chemistry and Materials Science, University of Szeged, Aradi vértanúk tere 1, Szeged, H-6720, Hungary.
‡adewit@ulb.ac.be

[1] J. D. Murray, *Mathematical Biology* (Springer Verlag, Berlin, 2003).
[2] V. Volpert and S. Petrovskii, Phys. Life Rev. **6**, 267 (2009).
[3] J. V. Noble, Nature (London) **250**, 726 (1974).
[4] R. M. Anderson and R. M. May, *Infectious Diseases in Humans: Dynamics and Control* (Oxford University Press, Oxford, 1991).
[5] S. Kondo and T. Miura, Science **329**, 1616 (2010).
[6] J. Weickert, *Anisotropic Diffusion in Image Processing* (Teubner-Verlag, Leipzig, 1998).
[7] B. A. Grzybowski, *Chemistry in Motion* (Wiley & Sons, New York, 2009).
[8] I. R. Epstein and B. Xu, Nat. Nanotechnol. **11**, 312 (2016).
[9] H. K. Henisch, *Periodic Precipitation* (Pergamon Press, New York, 1991).
[10] P. J. Ortoleva, *Geochemical Self-Organization* (Oxford University Press, Oxford, 1994).
[11] I. Mastromatteo, B. Tóth, and J.-P. Bouchaud, Phys. Rev. Lett. **113**, 268701 (2014).
[12] D. Toussaint and F. Wilczek, J. Chem. Phys. **78**, 2642 (1983).
[13] L. Gálfi and Z. Rácz, Phys. Rev. A **38**, 3151 (1988).
[14] Z. Jiang and C. Ebner, Phys. Rev. A **42**, 7483 (1990).
[15] Y. E. Koo, L. Li, and R. Kopelman, Mol. Cryst. Liq. Cryst. **183**, 187 (1990).
[16] Y.-E. L. Koo and R. Kopelman, J. Stat. Phys. **65**, 893 (1991).
[17] S. H. Park, S. Parus, R. Kopelman, and H. Taitelbaum, Phys. Rev. E **64**, 055102(R) (2001).
[18] F. A. Williams, *Combustion Theory* (Benjamin-Cummings, New York, 1985).
[19] J. H. Seinfeld and S. N. Pandis, *Atmospheric Chemistry and Physics* (Wiley & Sons, New York, 2006).
[20] A. Okubo and S. A. Levin, *Diffusion and Ecological Problems* (Springer Verlag, Berlin, 2001).
[21] R. S. Cantrell and C. Cosner, *Spatial Ecology via Reaction-Diffusion Equations* (John Wiley & Sons Ltd., Chichester, 2003).
[22] E. R. Abraham, Nature (London) **391**, 577 (1998).
[23] L. Rongy, P. M. J. Trevelyan, and A. De Wit, Phys. Rev. Lett. **101**, 084503 (2008).
[24] A. De Wit, Phil. Trans. R. Soc. A **374**, 20150419 (2016).
[25] J. M. Matter *et al.*, Science **352**, 1312 (2016).
[26] F. Haudin, J. H. E. Cartwright, F. Brau, and A. De Wit, Proc. Natl. Acad. Sci. U.S.A. **111**, 17363 (2014).
[27] F. Haudin, V. Brasiliense, J. H. E. Cartwright, F. Brau, and A. De Wit, Phys. Chem. Chem. Phys. **17**, 12804 (2015).
[28] G. Schuszter, F. Brau, and A. De Wit, Environ. Sci. Technol. Lett. **3**, 156 (2016).
[29] G. Schuszter, F. Brau, and A. De Wit, Phys. Chem. Chem. Phys. **18**, 25592 (2016).
[30] B. Bohner, G. Schuszter, O. Berkesi, D. Horváth, and Á. Tóth, Chem. Commun. (Cambridge) **50** (2014) 4289.
[31] P. Pusztai, E. Tóth-Szeles, D. Horváth, Á. Tóth, Á. Kukovecz, and Z. Kónya, Cryst. Eng. Commun. **17**, 8477 (2015).
[32] B. Bohner, G. Schuszter, D. Horváth, and Á. Tóth, Chem. Phys. Lett. **631**, 114 (2015).
[33] B. Bohner, B. Endrődi, D. Horváth, and Á. Tóth, J. Chem. Phys. **144**, 164504 (2016).
[34] E. Tóth-Szeles, G. Schuszter, Á. Tóth, Z. Kónya, and D. Horváth, Cryst. Eng. Commun. **18**, 2057 (2016).
[35] D. Brockmann and D. Helbing, Science **342**, 1337 (2013).
[36] Z. Koza, J. Stat. Phys. **85**, 179 (1996).
[37] F. W. J. Olver, D. W. Lozier, R. F. Boisvert, and C. W. Clark, *NIST Handbook of Mathematical Functions* (Cambridge University Press, New York, 2010); see also http://dlmf.nist.gov.
[38] See Supplemental Material http://link.aps.org/supplemental/10.1103/PhysRevLett.118.134101, which include Refs. [39–41], for the properties of K, the evolution of I_{tot} for $\gamma = 1/2$ and 2, the particle size and nearest neighbor distributions, and the details of the front position analysis.
[39] N. M. Temme, Math. Comp. **58**, 755 (1992).
[40] H. Taitelbaum, S. Havlin, J. E. Kiefer, B. Trus, and G. H. Weiss, J. Stat. Phys. **65**, 873 (1991).
[41] O. Velts, M. Uibu, J. Kallas, and R. Kuusik, Energy Procedia **4**, 771 (2011).
[42] F. Haudin and A. De Wit, Phys. Fluids **27**, 113101 (2015).
[43] Y. Nagatsu, Y. Ishii, Y. Tada, and A. De Wit, Phys. Rev. Lett. **113**, 024502 (2014).